Title

Equilibrium configuration of a bounded inextensible membrane subject to solar radiation pressure

Authors

Fu, Bo
Farouki, Rida T
Eke, Fidelis O

Publication Date

2017-09-01

DOI

10.1016/j.ast.2017.06.018

Peer reviewed

Equilibrium configuration of a bounded inextensible membrane subject to solar radiation pressure

Bo Fu, Rida T. Farouki, and Fidelis O. Eke
Department of Mechanical and Aerospace Engineering,
University of California, Davis, CA 95616.

Abstract

The equilibrium shape of a thin inextensible membrane subject to solar radiation pressure under given boundary constraints is studied. The membrane is assumed to be insusceptible to elastic deformation and to have negligible bending resistance, and its steady–state shape is therefore described by a developable surface (i.e., a surface of zero Gaussian curvature), resulting from an equilibrium between radiation pressure and membrane tension forces. A quantitative understanding of the mechanics of such membranes is essential in characterizing the dynamics of solar sail spacecraft that use sail wing tip displacement as an attitude control mode. The analysis in this paper develops a theoretical foundation for the billowed wing shape. Under reasonable simplifying assumptions, the key result is that solar radiation pressure and a given wing tip displacement yield a billowed solar sail wing with the shape of a generalized cylinder (i.e., a developable ruled surface, whose rulings are all parallel, rather than a general developable with variable ruling directions). The base curve geometry for the solar sail is also determined as the solution to a boundary value problem. The results presented herein allow the shape of the billowed membrane to be computed to any desired precision, for any given tip displacement.

Keywords: solar sails; inextensible membranes; developable surfaces; elliptic integrals; numerical quadrature; boundary value problem.

e–mail: bofu@ucdavis.edu, farouki@ucdavis.edu, foeke@ucdavis.edu

1 Introduction

Solar sails differ from traditional spacecraft in that they harvest momentum from solar radiation pressure, rather than expulsion of onboard propellants. This property of solar sails can significantly reduce mass–to–orbit, especially for round–trip missions requiring a spacecraft to carry return fuel on launch. This results is greatly improved mission cost effectiveness, making solar sails promising candidates for future interplanetary space transportation [15].

Although interest in solar sail technology has grown within the last decade, following the successful demonstration of solar sail technology by the Japanese IKAROS [19] mission in 2010 and also the recent Lightsail–1 mission by the Planetary Society in 2015, the technology is still in a rudimentary state of development. Most solar sail studies have thus far focused on small sails. However, the idea of large solar sails is not new [2, 3, 4, 9, 13, 21]. Large sails have the potential to carry payloads up to several metric tons, and could be the key to cost–effective space cargo transportation.

Attitude control remains a critical area of interest in the exploitation of solar sail technology. This is because attitude control for solar sails requires methodologies fundamentally different from those employed by traditional spacecraft. A deployed solar sail will require continuous attitude correction, due to the misalignment of the sail center of pressure (cp) and the sail center of mass (cm). The cm–cp misalignment results from both manufacturing and deployment imperfections, and thus cannot be avoided. The large moment of inertia of a deployed solar sail will also require large body moments for attitude maneuvers, limiting the use of traditional attitude control methods. The reader may consult the paper [20] by Wie for a more detailed discussion of the limitations of traditional attitude control methods in solar sails.

For a solar sail, it makes sense to use solar radiation pressure (SRP) as the *only* source for attitude control moment generation. This can be done by manipulating the cm and cp positions on the sail. Most attitude control methods proposed for solar sails require the addition of substantial mass to the craft as the sail size increases. Recently, an attitude control methodology was proposed by Fu and Eke [7] that does not require significant additional mass. This approach employs a square solar sail, as shown in Figure 1.

The square sail consists of four right triangular wings, connected to the support booms only at their tips and at the center. For example, in Figure 1 wing A is attached to the support booms at points O, P, and Q. The basic idea is to displace the sail membrane–boom attachment point, such as point

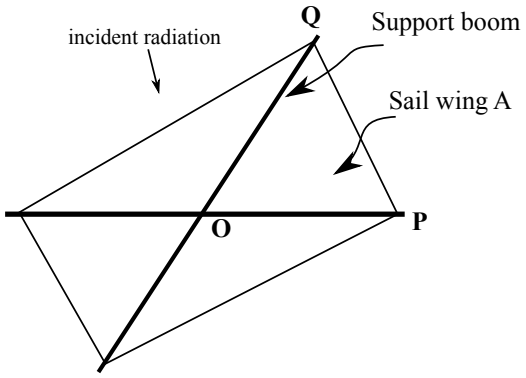

Figure 1: Schematics of square solar sail

P, a distance δ toward the center O, so that the membrane billows under solar radiation pressure. This billowing of the sail membrane causes a shift in both the membrane cm and cp, which in turn induces a body torque that can be exploited for attitude control. Simultaneous displacements of more than one of the four wing tips in a square solar sail allow body moments to be generated about all three body axis directions. The reader may consult [7] for a more detailed description of the method, which will be referred to as the Tip Displacement Method (TDM) of attitude control.

An accurate estimate of the shape of the billowed sail wing under a given tip displacement is critical in the effective application of TDM in solar sail attitude control, since the SRP forces and torques are a direct result of the billowed shape. Several authors [10, 11, 17, 22] have proposed methods to estimate the deformed shapes and resulting total forces on solar sails, using a variety of approaches. The analysis in [7] was based upon some reasonable assumptions concerning the shape of the deformed membrane, to facilitate estimation of the resulting attitude torques. The main assumption is that the shape of the billowed wing is a portion of a right circular cylinder. A more rigorous study, that does not invoke the right circular cylinder assumption, was conducted by Fu and Eke [8]. By means of a numerical optimization method, it was found that the billowed wing shape differs from a cylindrical shape, but for small tip displacements this deviation is small and a cylindrical shape is sufficient for attitude torque estimations.

Although the studies [7] and [8] extended knowledge of the TDM and billowed wing profile, a sound theoretical basis for understanding the billowed wing shape was lacking. In [7], the shape was assumed to be cylindrical, and

in reference [8], the shape was assumed to be a generalized cylinder, with the base curve obtained numerically via an optimization algorithm. This paper provides a deeper understanding of the wing profile through a first–principles approach to the mechanics of bounded inextensible membranes, and a rigorous method of solving the boundary value problem that determines the equilibrium shape of the sail wing base curve, for any given wing tip displacement. The sail wing is modeled as an inextensible membrane, whose billowed shape is determined by equilibration of solar radiation pressure and internal membrane stresses, upon imposing membrane boundary conditions — namely, the displacement of one wing tip.

Although many aspects of plate and membrane mechanics have previously been studied in depth [1, 5, 6, 12, 14, 16], the authors are unaware of any prior detailed investigation of the specific problem addressed herein, concerning the equilibrium shape of an initially flat membrane that is inextensible but offers no bending resistance, and billows under the action of uniform pressure when one tip is displaced. The deformed shape of an inextensible membrane must be a *developable*, i.e., a ruled surface of zero Gaussian curvature [18]. A developable surface may be a *cylinder* (whose rulings are all parallel); a *cone* (whose rulings all pass through a fixed point); or a *tangent developable* (the surface generated by the family of tangent lines to a given space curve — the most general case). Through a detailed investigation of the force and torque equilibrium of a differential membrane surface element, it is shown in this paper that the billowed sail necessarily assumes the shape of a (generalized) cylinder, i.e., the surface generated by a family of parallel lines emanating from a given "base" curve.

2 Kinematics of a solar sail wing

As noted above, a deformed inextensible membrane assumes the shape of a developable surface, a special type of ruled surface that can be *developed* [18] or "flattened" by pure bending action, without any stretching/compressing. The development process preserves distances, angles, and surface areas.

Consider a billowed inextensible solar sail wing, as shown in Figure 2. If the sail boundary OP is described by a "base curve" $\mathbf{c}(s)$, the sail surface admits a parameterization of the form

$$\mathbf{r}(s,t) \;=\; \mathbf{c}(s) + t\,\mathbf{d}(s)\,, \tag{1}$$

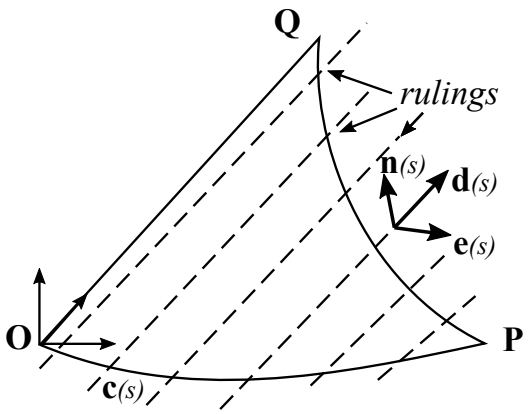

Figure 2: Billowed sail wing

where $\mathbf{d}(s)$ is a unit vector specifying the ruling direction at each point of $\mathbf{c}(s)$ and t is distance along the ruling originating from $\mathbf{c}(s)$. Inextensibility of the curve $\mathbf{c}(s)$ is enforced by assuming an arc–length parameterization, i.e.,

$$|\mathbf{c}'(s)| \equiv 1. \tag{2}$$

Note that arc–length parameterization is common in describing inextensible objects, such as ropes or chains.

Expression (1) describes a general ruled surface, which is not necessarily developable. To define a developable surface, appropriate to the context of an inextensible solar sail membrane, the arc–length parameterization condition (2) is not sufficient, and we must impose another condition which ensures that $\mathbf{r}(s,t)$ has zero Gaussian curvature. The Gaussian curvature of a parametric surface can be determined [18] as follows (for brevity, we henceforth omit the dependence of $\mathbf{c}$ and $\mathbf{d}$ and their derivatives $\mathbf{c}', \mathbf{c}''$ and $\mathbf{d}', \mathbf{d}''$ on s). The first partial derivatives of $\mathbf{r}(s,t)$ are

$$\mathbf{r}_s \,=\, \mathbf{c}' + t\,\mathbf{d}'\,, \qquad \mathbf{r}_t \,=\, \mathbf{d}\,,$$

and, if they are linearly independent, the unit surface normal is specified by

$$\mathbf{n} \,=\, \frac{\mathbf{r}_s \times \mathbf{r}_t}{|\mathbf{r}_s \times \mathbf{r}_t|} \,=\, \frac{(\mathbf{c}' + t\,\mathbf{d}') \times \mathbf{d}}{|(\mathbf{c}' + t\,\mathbf{d}') \times \mathbf{d}|}\,.$$

Now since $|\mathbf{d}| = 1$ and $\mathbf{d} \cdot \mathbf{d}' = 0$, the first fundamental form of $\mathbf{r}(s,t)$ has the coefficients

$$E \,:=\, \mathbf{r}_s \cdot \mathbf{r}_s \,=\, |\mathbf{c}' + t\,\mathbf{d}'|^2\,, \quad F \,:=\, \mathbf{r}_s \cdot \mathbf{r}_t \,=\, \mathbf{c}' \cdot \mathbf{d}\,, \quad G \,:=\, \mathbf{r}_t \cdot \mathbf{r}_t \,=\, 1\,.$$

Similarly, the second partial derivatives of $\mathbf{r}(s,t)$ are

$$\mathbf{r}_{ss} \,=\, \mathbf{c}'' + t\,\mathbf{d}''\,, \quad \mathbf{r}_{st} \,=\, \mathbf{d}'\,, \quad \mathbf{r}_{tt} \,=\, \mathbf{0}\,,$$

and the second fundamental form has the coefficients

$$L \,=\, \mathbf{n}\cdot\mathbf{r}_{ss}\,, \quad M \,=\, \mathbf{n}\cdot\mathbf{r}_{st}\,, \quad N \,=\, \mathbf{n}\cdot\mathbf{r}_{tt} \,=\, 0\,.$$

The Gaussian curvature K of $\mathbf{r}(s,t)$ is defined in terms of the first and second fundamental form coefficients as

$$K \,=\, \frac{LN - M^2}{EG - F^2}\,,$$

and the condition $K \equiv 0$ is sufficient and necessary for a developable surface. In the present context, this condition becomes

$$[\,(\mathbf{c}' + t\,\mathbf{d}')\times\mathbf{d}\,]\cdot\mathbf{d}' \,\equiv\, 0\,,$$

which reduces to

$$\mathbf{c}'\cdot(\mathbf{d}\times\mathbf{d}') \,\equiv\, 0\,. \tag{3}$$

Equation (3) states that, for a developable surface, the base curve $\mathbf{c}$ and ruling direction $\mathbf{d}$ are related, and cannot be arbitrarily specified. Defining a unit vector $\mathbf{e}$

$$\mathbf{e} \,:=\, \frac{\mathbf{d}'}{|\mathbf{d}'|} \tag{4}$$

in the direction of the derivative $\mathbf{d}'$ of the ruling vector, equation (3) can be expressed as

$$\mathbf{c}'\cdot(\mathbf{d}\times\mathbf{e}) \,\equiv\, 0\,, \tag{5}$$

i.e., $\mathbf{c}'$ is linearly dependent on $\mathbf{d}$ and $\mathbf{e}$. Since $\mathbf{d}$ and $\mathbf{e}$ are orthogonal, and span the surface tangent plane, the unit surface normal vector $\mathbf{n}$ may be written as

$$\mathbf{n} \,=\, \mathbf{e}\times\mathbf{d}\,. \tag{6}$$

Note that $\mathbf{n}$ depends only on s, i.e., it is constant along each ruling — in fact, this can be regarded as a geometrical property that distinguishes developable from non–developable ruled surfaces. The introduction of the unit vector $\mathbf{e}$ in the direction of $\mathbf{d}'$ helps to simplify the analysis of the membrane mechanics, as will be seen in the following section.

3 Mechanics of solar sail wing

The analysis of the solar sail wing mechanics will be based on the simplifying assumptions enumerated below. The intent is to formulate a basic analytical model, which may serve as the point of departure for studying higher–order effects (such as inclusion of non–zero shear stresses, finite bending stiffness, or load–dependent stiffness).

(a) The sail membrane material is inextensible, and hence the geometrical form of the billowed wing is governed by equation (5).

(b) The membrane material cannot carry any torsional or bending load, a reasonable assumption for sails with a large ratio of area to thickness (area/thickness $\sim 10^{10}$ for the large solar sail considered in [7, 8]).

(c) Shear stresses in the membrane are considered to be negligible — the dominant stress being a direct stress orthogonal to the rulings, with a constant magnitude along each ruling.

(d) The solar radiation pressure (SRP) is calculated on the basis of specular reflection from the membrane, a common assumption in a first analysis.

However, there are no *a priori* assumptions concerning the variation of the ruling direction $\mathbf{d}$. It should be noted that assumption (c) must be invalid along the edge OQ in Figure 2 if the sail is attached to the support boom at only the two points O and Q. At some distance from this edge, however, it may offer a reasonable approximation to the actual membrane stress state.

3.1 Force equilibrium

Based on the above assumptions, the only forces exerted on the sail wing are the SRP force and tensile forces orthogonal to the rulings. The SRP force $\mathbf{F}_{SRP}$ incurred by pure specular reflection from a sail area element $\mathrm{d}A$ acts in the direction of the surface normal $\mathbf{n}$, and may be expressed as

$$\mathbf{F}_{SRP} \;=\; -\,P_0\,(\mathbf{n}\cdot\mathbf{s})^2\,\mathbf{n}\,\mathrm{d}A\,,$$

where $\mathbf{s}$ is a unit vector in the direction of the incident radiation and P_0 is the nominal SRP (i.e., when $\mathbf{s}$ is parallel to $\mathbf{n}$) at the sail location. For an interplanetary solar sail that is not too close to the sun, the incident radiation

is assumed to be uniform, with P_0 and $\mathbf{s}$ constant for any given time and sail location. Since the surface normal $\mathbf{n}$ is constant along each ruling, it suffices to consider a differential area element $\mathrm{d}A$ between two rulings that correspond to parameter values s and $s + \mathrm{d}s$ along the base curve $\mathbf{c}(s)$.

Consider a wing element $ABCD$ between two rulings (see Figure 3). The vector function defined by

$$\mathbf{l}(s) \,:=\, l(s)\,\mathbf{d}(s) \tag{7}$$

is introduced, $l(s)$ being the length of the ruling emanating from the point $\mathbf{c}(s)$ on the base curve (it is not necessary to precisely specify $l(s)$ for the following analysis). The differential area element $\mathrm{d}A$ can be found as follows. To first order in $\mathrm{d}s$, the corner points A, B, C, D have the locations

$$\mathbf{r}_A \,=\, \mathbf{c}\,, \quad \mathbf{r}_B \,=\, \mathbf{c} + \mathbf{c}'\mathrm{d}s\,, \quad \mathbf{r}_C \,=\, \mathbf{c} + \mathbf{c}'\mathrm{d}s + \mathbf{l} + \mathbf{l}'\mathrm{d}s\,, \quad \mathbf{r}_D \,=\, \mathbf{c} + \mathbf{l}\,,$$

Thus the vectors $\vec{AC}$ and $\vec{BD}$ are

$$\vec{AC} = \mathbf{r}_C - \mathbf{r}_A \,=\, \mathbf{c}'\mathrm{d}s + \mathbf{l} + \mathbf{l}'\mathrm{d}s\,, \qquad \vec{BD} = \mathbf{r}_D - \mathbf{r}_B \,=\, \mathbf{l} - \mathbf{c}'\mathrm{d}s\,.$$

Now by equation (3), the scalar triple product

$$\vec{AB} \cdot (\vec{AD} \times \vec{BC}) \,=\, \mathbf{c}' \cdot (\mathbf{d} \times \mathbf{d}')\, l^2 (\mathrm{d}s)^2$$

vanishes, so the differential surface element $ABCD$ is a planar quadrilateral to the first order in $\mathrm{d}s$.

The area of the differential surface element is then given, to first order in $\mathrm{d}s$, by

$$\mathrm{d}A \,=\, \tfrac{1}{2}\,|\,\vec{AC} \times \vec{BD}\,| \,=\, \tfrac{1}{2}\,|\,(\mathbf{l}+\mathbf{c}'\mathrm{d}s+\mathbf{l}'\mathrm{d}s)\times(\mathbf{l}-\mathbf{c}'\mathrm{d}s)\,| \,=\, |(\mathbf{c}'\times\mathbf{l}+\tfrac{1}{2}\,\mathbf{l}'\times\mathbf{l})|\,\mathrm{d}s\,.$$

Introducing the scalar quantity $P := P_0(\mathbf{n}\cdot\mathbf{s})^2$ and the vector area element

$$\mathrm{d}\mathbf{A} \,:=\, \mathbf{n}\,\mathrm{d}A \,=\, (\mathbf{c}' \times \mathbf{l} + \tfrac{1}{2}\,\mathbf{l}' \times \mathbf{l})\,\mathrm{d}s\,,$$

the SRP force on the differential membrane strip can be written as

$$\mathbf{F}_{SRP} \,=\, -\,P\,\mathrm{d}\mathbf{A} \,=\, -\,P\,(\mathbf{c}' \times \mathbf{l} + \tfrac{1}{2}\,\mathbf{l}' \times \mathbf{l})\,\mathrm{d}s\,. \tag{8}$$

Let $\sigma(s)$ denote the product of the membrane thickness and the tensile normal stress along the ruling $\mathbf{l}(s)$, as shown in Figure 3. Since the stress

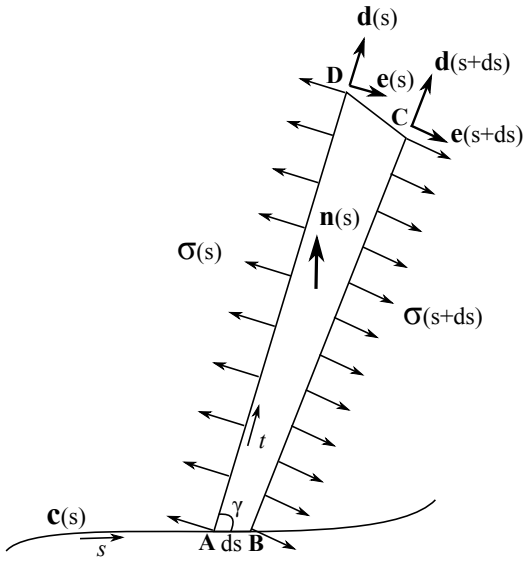

Figure 3: Differential membrane strip bounded by two surface rulings

is always in the direction of $\mathbf{e}$, and uniform along each ruling, we can define a tension vector $\mathbf{T}(s) := \sigma(s)l(s)\mathbf{e}(s)$. The tension forces on the edges AD and BC of the differential area element are then

$$\mathbf{F}_{AD} \,=\, -\,\mathbf{T}(s) \qquad \text{and} \qquad \mathbf{F}_{BC} \,=\, \mathbf{T}(s+\mathrm{d}s) \,=\, \mathbf{T}(s) + \mathbf{T}'(s)\,\mathrm{d}s\,. \tag{9}$$

Thus, in steady state equilibrium, from (8) and (9) we must have

$$\mathbf{F}_{BC} + \mathbf{F}_{AD} + \mathbf{F}_{SRP} \,=\, \mathbf{T} + \mathbf{T}'\mathrm{d}s - \mathbf{T} - P(\mathbf{c}' \times \mathbf{l} + \tfrac{1}{2}\,\mathbf{l}' \times \mathbf{l})\mathrm{d}s \,=\, \mathbf{0}\,.$$

Dividing by $\mathrm{d}s$ then gives the steady state force equilibrium condition

$$\mathbf{T}' \,=\, P(\mathbf{c}' \times \mathbf{l} + \tfrac{1}{2}\,\mathbf{l}' \times \mathbf{l})\,. \tag{10}$$

This states that the change in tension force between two consecutive rulings is proportional to the external SRP force P and the surface area bounded by those rulings, and its direction coincides with the surface normal.

When the base curve $\mathbf{c}(s)$ is constrained to be planar and the rulings $\mathbf{l}(s)$ are orthogonal to the plane containing it, equation (10) reduces to the well–known equilibrium equation for a one–dimensional inextensible chain [23]. Equation (10) can thus be regarded as a two–dimensional generalization of the inextensible chain equation. However, equation (10) alone is not sufficient to characterize the equilibrium membrane mechanics: moments acting on the membrane must also be considered.

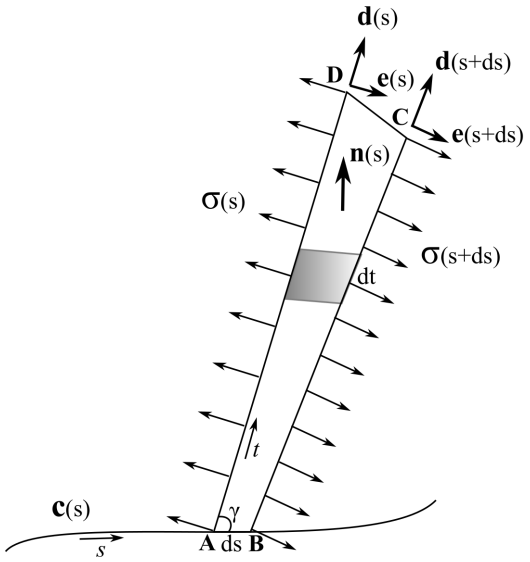

Figure 4: Sub–element of differential strip bounded by two surface rulings

3.2 Moment equilibrium

Consider a sub–element of a differential strip bounded by rulings emanating from the points $\mathbf{c}(s)$ and $\mathbf{c}(s + \mathrm{d}s)$ of the base curve, that corresponds to an increment $\mathrm{d}t$ in the ruling parameter (indicated by the shaded region in Figure 4). The vector area of this sub–element is given by [18]

$$\sqrt{EG - F^2}\,\mathbf{n}\,\mathrm{d}s\,\mathrm{d}t \;=\; |\mathbf{r}_s \times \mathbf{r}_t|\,\mathbf{n}\,\mathrm{d}s\,\mathrm{d}t \;=\; (\mathbf{c}' \times \mathbf{d} + t\,\mathbf{d}' \times \mathbf{d})\,\mathrm{d}s\,\mathrm{d}t\,.$$

Let the center of pressure on this sub–element be identified by displacement $\mathrm{d}\mathbf{r}$ relative to the point $\mathbf{r}(s,t) = \mathbf{c}(s) + t\,\mathbf{d}(s)$. Then the total SRP moment on the differential strip about point A can be formulated as an integral with respect to t, namely

$$\mathbf{M}_{SRP} \;=\; \int_0^l [\,t\,\mathbf{d} + \mathrm{d}\mathbf{r}\,] \times [\,-P\,(\mathbf{c}' \times \mathbf{d} + t\,\mathbf{d}' \times \mathbf{d})\,\mathrm{d}s\,\mathrm{d}t\,]\,.$$

Since $\mathrm{d}\mathbf{r}$ and $\mathrm{d}s$ are infinitesimals of the same order, to first order in $\mathrm{d}s$ this becomes

$$\mathbf{M}_{SRP} \;=\; -\,[\,\tfrac{1}{2}Pl^2\mathbf{d} \times (\mathbf{c}' \times \mathbf{d}) + \tfrac{1}{3}Pl^3\mathbf{d} \times (\mathbf{d}' \times \mathbf{d})\,]\,\mathrm{d}s\,. \qquad (11)$$

The tension forces on edges AD and BC also exert moments about point A. The total moment generated by tensile forces along edge AD can be expressed as an integral with respect to t,

$$\mathbf{M}_{AD} \;=\; \int_0^l t\,\mathbf{d}\times(-\sigma\mathbf{e})\,\mathrm{d}t\,, \tag{12}$$

Since the ruling direction $\mathbf{d}$, tensile stress σ, and directional vector $\mathbf{e}$ depend only on the arc length s, the integral in (12) can be directly evaluated from 0 to l to give

$$\mathbf{M}_{AD} \;=\; -\tfrac{1}{2}\,l^2\,\sigma\,\mathbf{d}\times\mathbf{e}\,. \tag{13}$$

Similarly, the total moment generated by tensile forces along edge BC can be expressed by an integral with respect to t with integration limits 0 and $l(s+\mathrm{d}s)$,

$$\mathbf{M}_{BC} \;=\; \int_0^{l(s+\mathrm{d}s)} [\,\mathbf{c}'\mathrm{d}s + t\,\mathbf{d}(s+\mathrm{d}s)\,]\times[\,\sigma(s+\mathrm{d}s)\mathbf{e}(s+\mathrm{d}s)\,]\,\mathrm{d}t\,. \tag{14}$$

Now exact expressions for functions of the form $f(s+\mathrm{d}s)$, such as the upper integration limit $l(s+\mathrm{d}s)$, ruling direction $\mathbf{d}(s+ds)$, etc., are unknown. To evaluate (14), one can invoke the first order approximation $f(s+ds) = f(s)+f'(s)\mathrm{d}s$, and decompose the integral in (14) into two parts: from 0 to l, and from l to $l+l'\mathrm{d}s$. This gives

$$\begin{aligned}\mathbf{M}_{BC} \;=\; &\int_0^{l} [\,\mathbf{c}'\mathrm{d}s + t(\mathbf{d}+\mathbf{d}'\mathrm{d}s)\,]\times[\,(\sigma+\sigma'\mathrm{d}s)(\mathbf{e}+\mathbf{e}'\mathrm{d}s)\,]\,\mathrm{d}t\\ &+\int_l^{l+l'\mathrm{d}s} [\,\mathbf{c}'\mathrm{d}s + t(\mathbf{d}+\mathbf{d}'\mathrm{d}s)\,]\times[\,(\sigma+\sigma'\mathrm{d}s)(\mathbf{e}+\mathbf{e}'\mathrm{d}s)\,]\,\mathrm{d}t\,.\end{aligned} \tag{15}$$

Evaluating each part with respect to its integration limits gives, to first order in $\mathrm{d}s$,

$$\mathbf{M}_{BC} \;=\tfrac{1}{2}\,l^2\,\sigma\,\mathbf{d}\times\mathbf{e} + [\,\sigma l\,\mathbf{c}'\times\mathbf{e} + \tfrac{1}{2}l^2(\sigma\mathbf{d}\times\mathbf{e})' + ll'\sigma\mathbf{d}\times\mathbf{e}\,]\,\mathrm{d}s\,. \tag{16}$$

The last two terms on the right in equation (16) can be further combined into a total derivative,

$$\mathbf{M}_{BC} \;=\tfrac{1}{2}\,l^2\,\sigma\,\mathbf{d}\times\mathbf{e} + [\,\sigma l\,\mathbf{c}'\times\mathbf{e} + (\tfrac{1}{2}l^2\sigma\mathbf{d}\times\mathbf{e})'\,]\,\mathrm{d}s\,. \tag{17}$$

From equations (11), (13), and (17) we can sum the moments about point A — after simplifying, we obtain

$$\mathbf{M}_{BC} + \mathbf{M}_{AD} + \mathbf{M}_{SRP} = [\, \sigma l\, \mathbf{c}' \times \mathbf{e} + \tfrac{1}{2} l^2 (\sigma \mathbf{d} \times \mathbf{e})' + l l' \sigma \mathbf{d} \times \mathbf{e} - \tfrac{1}{2} P\, l^2 \mathbf{d} \times (\mathbf{c}' \times \mathbf{d}) - \tfrac{1}{3} P\, l^3 \mathbf{d} \times (\mathbf{d}' \times \mathbf{d})\,] \, \mathrm{d}s\,.$$

Setting $\mathbf{T} = \sigma\, l\, \mathbf{e}$, this reduces to

$$\mathbf{M}_{BC} + \mathbf{M}_{AD} + \mathbf{M}_{SRP} \;=\; [\, \mathbf{c}' \times \mathbf{T} + \tfrac{1}{2} (\mathbf{l} \times \mathbf{T})' - \tfrac{1}{2} P\, \mathbf{l} \times (\mathbf{c}' \times \mathbf{l}) - \tfrac{1}{3} P\, l^3 \mathbf{d} \times (\mathbf{d}' \times \mathbf{d})\,] \, \mathrm{d}s\,.$$

Setting the above expression to zero, the condition for moment equilibrium of a bounded inextensible membrane at steady state is

$$2\mathbf{c}' \times \mathbf{T} + (\mathbf{l} \times \mathbf{T})' - P\, \mathbf{l} \times (\mathbf{c}' \times \mathbf{l}) - \tfrac{2}{3} P\, \mathbf{l} \times (l \mathbf{d}' \times \mathbf{l}) \;=\; \mathbf{0}\,. \qquad (18)$$

The first and second terms in (18) represent moments generated by tensile stresses, while the third and fourth represent moments generated by the SRP. Note that the SRP moments are always in the direction of $-\mathbf{e}$, since

$$\mathbf{l} \times (\mathbf{c}' \times \mathbf{l}) \;=\; \mathbf{l} \times (|\mathbf{c}'|\, |\mathbf{l}| \sin\gamma\, \mathbf{n}) \;=\; |\mathbf{c}'|\, |\mathbf{l}|^2 \sin\gamma\, \mathbf{e} \;=\; l^2 \sin\gamma\, \mathbf{e}\,,$$

where γ is the angle formed by the base curve $\mathbf{c}$ and the ruling direction $\mathbf{d}$ (as shown in Figure 4), and

$$\mathbf{d} \times (\mathbf{d}' \times \mathbf{d}) \;=\; \mathbf{d}' \;=\; |\mathbf{d}'|\, \mathbf{e}\,.$$

In summary, the billowed sail wing must satisfy equations (5), (10), and (18) in the steady state.

4 Inextensible sail wing under SRP

In the solar sail tip–displacement attitude control method, the billowed sail shape directly affects the induced attitude torque. However, a first–principles analysis of the actual sail shape induced by SRP has not yet been performed. It has been intuitively supposed that the billowed wing will assume the form of a generalized cylinder, and this was invoked as a "reasonable" assumption in prior studies [7, 8]. However, as shown below, a formal justification for this supposition — based on a quantitative analysis of the sail mechanics — is a non–obvious and non–trivial task. The preceding results lay the foundation

for a more rigorous analysis of the precise sail shape. Based on these results, it is now shown that (under the stated assumptions) the shape of a billowed sail wing subject to SRP and a given tip displacement does indeed assume the form of a generalized cylinder.

The argument proceeds as follows. Equation (18) is equivalent to

$$2\mathbf{c}' \times \mathbf{T} + \mathbf{l}' \times \mathbf{T} + \mathbf{l} \times \mathbf{T}' - P\,\mathbf{l} \times (\mathbf{c}' \times \mathbf{l}) - \tfrac{2}{3} P\, l^3 \mathbf{d}' \;=\; \mathbf{0}\,.$$

Substituting from equation (10) then gives

$$2\mathbf{c}' \times \mathbf{T} + \mathbf{l}' \times \mathbf{T} + P\,\mathbf{l} \times (\mathbf{c}' \times \mathbf{l} + \tfrac{1}{2}\mathbf{l}' \times \mathbf{l}) - P\,\mathbf{l} \times (\mathbf{c}' \times \mathbf{l}) - \tfrac{2}{3} P\, l^3 \mathbf{d}' \;=\; \mathbf{0}\,,$$

which reduces to

$$2\mathbf{c}' \times \mathbf{T} + \mathbf{l}' \times \mathbf{T} + \tfrac{1}{2} P\,\mathbf{l} \times (\mathbf{l}' \times \mathbf{l}) - \tfrac{2}{3} P\, l^3 \mathbf{d}' \;=\; \mathbf{0}\,,$$

or, on expanding the vector triple product,

$$2\mathbf{c}' \times \mathbf{T} + \mathbf{l}' \times \mathbf{T} + \tfrac{1}{2} P\,[\, l^2 \mathbf{l}' - (\mathbf{l} \cdot \mathbf{l}')\mathbf{l}\,] - \tfrac{2}{3} P\, l^3 \mathbf{d}' \;=\; \mathbf{0}\,. \tag{19}$$

Next, taking the dot product of (19) with $\mathbf{c}'$ and noting that $\mathbf{c}' \cdot (\mathbf{c}' \times \mathbf{T}) = 0$, this becomes

$$\mathbf{c}' \cdot (\mathbf{l}' \times \mathbf{T}) + \tfrac{1}{2} P\,[\, l^2 (\mathbf{c}' \cdot \mathbf{l}') - (\mathbf{l} \cdot \mathbf{l}')(\mathbf{c}' \cdot \mathbf{l})\,] - \tfrac{2}{3} P\, l^3 (\mathbf{c}' \cdot \mathbf{d}') \;=\; 0\,. \tag{20}$$

From (7), we substitute $\mathbf{l} = l\,\mathbf{d}$ and $\mathbf{l}' = l'\mathbf{d} + l\,\mathbf{d}'$ into equation (20) and simplify to obtain

$$\mathbf{c}' \cdot (l'\mathbf{d} \times \mathbf{T}) + \mathbf{c}' \cdot (l\,\mathbf{d}' \times \mathbf{T}) + \tfrac{1}{2} P\, l^3 (\mathbf{c}' \cdot \mathbf{d}') - \tfrac{2}{3} P\, l^3 (\mathbf{c}' \cdot \mathbf{d}') \;=\; 0\,. \tag{21}$$

Since $\mathbf{T} = \sigma\, l\, \mathbf{e}$, the first term in equation (21) vanishes because of the developability condition (5). From the definition of the unit vector $\mathbf{e}$ in equation (4), the second term also vanishes. Thus, noting that $l \neq 0$ and $P \neq 0$, equation (21) reduces to

$$\mathbf{c}' \cdot \mathbf{d}' \;=\; 0\,. \tag{22}$$

Since the base curve $\mathbf{c}$ is parameterized by arc length, inextensibility implies that $|\mathbf{c}'(s)| \equiv 1$, i.e., $\mathbf{c}'$ is a unit vector, and the developability condition (5) indicates that $\mathbf{c}'$ must lie in the plane spanned by the unit vectors $\mathbf{d}$ and $\mathbf{e}$. Hence, there exists an angle $\gamma(s)$ such that

$$\mathbf{c}' \;=\; \cos\gamma\;\mathbf{d} \,\pm\, \sin\gamma\;\mathbf{e}\,. \tag{23}$$

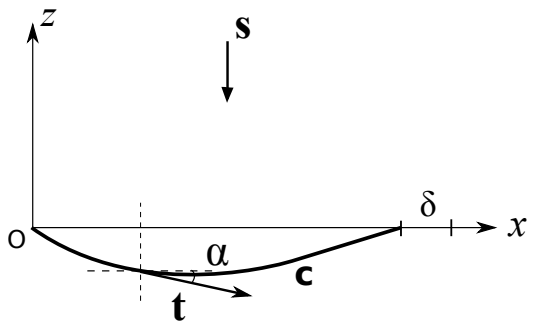

Figure 5: Side view of a billowed sail wing

Then, taking the dot product of equation (23) with $\mathbf{d}'$ and using equation (22) yields

$$\sin\gamma\,|\mathbf{d}'| \;=\; 0\,. \tag{24}$$

Now the angle $\gamma(s)$ remains invariant if the billowed sail wing is developed into a planar triangle, in which case $\gamma(0) = 90^\circ$ — i.e., the edges OP and OQ in Figure 1 are orthogonal. Hence, since $\sin\gamma \not\equiv 0$, equation (24) implies that $|\mathbf{d}'| = 0$, i.e.,

$$\mathbf{d}' \;=\; \mathbf{0}\,.$$

In other words, the ruling direction $\mathbf{d}$ is constant, and the billowed sail shape corresponds to a generalized cylinder. In particular, all rulings are parallel to the edge OQ in Figure 2.

5 Solution of the boundary value problem

When projected onto the (x, z) plane, a solar sail wing profile that is a generalized cylinder is simply the base curve $\mathbf{c}(s)$, as shown in Figure 5. For solar radiation pressure orthogonal to the wing, the steady state billowed wing profile is a result of the wing boundary conditions, that is, the amount of tip displacement δ. The following analysis allows the billowed wing base curve $\mathbf{c}(s)$ to be accurately determined for any given tip displacement δ.

The unit tangent to the base curve can be written as

$$\mathbf{t}(s) \;=\; (\cos\alpha(s), \sin\alpha(s))\,,$$

where $\alpha(s)$ is the angle it makes with positive x–direction, measured positive clockwise in the (x, z) plane (see Figure 5). It was shown in [8] that α is

related to the base curve arc length s by the expression

$$\tan\alpha \;=\; K_0(Ls - \tfrac{1}{2}\,s^2) + C_0\,, \tag{25}$$

where L is the total arc length, and K_0 and C_0 are constants to be determined from the boundary conditions. Interpreting this as a quadratic equation in s, it has the solution

$$s \;=\; L \pm \sqrt{L^2 - 2(\tan\alpha - C_0)/K_0}\,. \tag{26}$$

Let α_i and α_f be the initial and final tangent angles, at $s = 0$ and $s = L$. When $s = 0$ the expression on the right must vanish, and this is only possible if we choose the minus sign and

$$C_0 \;=\; \tan\alpha_i\,.$$

Similarly, when $s = L$ the radical term must vanish, and this gives

$$K_0 \;=\; \frac{2(\tan\alpha_f - \tan\alpha_i)}{L^2}\,.$$

Hence, the expression (26) can be re–written as

$$s \;=\; L\left[\,1 - \sqrt{1 - (\tau - \tau_i)/(\tau_f - \tau_i)}\,\right] \tag{27}$$

where, for brevity, we set

$$\tau \;=\; \tan\alpha\,, \quad \tau_i \;=\; \tan\alpha_i\,, \quad \tau_f \;=\; \tan\alpha_f\,.$$

Note that s is monotone–increasing for $\tau \in [\,\tau_i, \tau_f\,]$.

5.1 Boundary conditions

The sail base curve must satisfy the boundary constraints

$$\int_0^L \cos\alpha\;\mathrm{d}s \;=\; L - \delta\,, \qquad \int_0^L \sin\alpha\;\mathrm{d}s \;=\; 0\,.$$

Noting that

$$\cos\alpha \;=\; \frac{1}{\sqrt{1+\tau^2}}\,, \quad \sin\alpha \;=\; \frac{\tau}{\sqrt{1+\tau^2}}\,, \tag{28}$$

and using (27) to impose the changes of variables $s \to \tau$ with

$$\mathrm{d}s \;=\; \frac{L\,\mathrm{d}\tau}{2\sqrt{(\tau_f-\tau_i)(\tau_f-\tau)}}\,,$$

these conditions can be re–formulated as

$$\int_{\tau_i}^{\tau_f} \frac{\mathrm{d}\tau}{\sqrt{(\tau_f-\tau)(1+\tau^2)}} \;=\; 2\,\sqrt{\tau_f-\tau_i}\,(1-\delta/L)\,, \tag{29}$$

$$\int_{\tau_i}^{\tau_f} \frac{\tau\,\mathrm{d}\tau}{\sqrt{(\tau_f-\tau)(1+\tau^2)}} \;=\; 0\,. \tag{30}$$

The expressions on the left are *elliptic integrals* — i.e., integrals in which the integrand is rational in the integration variable τ and a single square root of a cubic or quartic expression in τ. Consider the indefinite integrals

$$\int \frac{\mathrm{d}\tau}{\sqrt{(\tau_f-\tau)(1+\tau^2)}} \qquad \text{and} \qquad \int \frac{\tau\,\mathrm{d}\tau}{\sqrt{(\tau_f-\tau)(1+\tau^2)}}\,.$$

They can be reduced to linear combinations of the standard forms

$$\mathcal{F}(k,\tau) = \int \frac{\mathrm{d}\tau}{\sqrt{(1-k^2\tau^2)(1-\tau^2)}} \quad \text{and} \quad \mathcal{E}(k,\tau) = \int \sqrt{\frac{1-k^2\tau^2}{1-\tau^2}}\;\mathrm{d}\tau\,,$$

known as elliptic integrals of the first and second kind, with parameter k. To accomplish this, the integration variable and parameter must be generalized to complex quantities. Specifically, we have

$$\int \frac{\mathrm{d}\tau}{\sqrt{(\tau_f-\tau)(1+\tau^2)}} \;=\; \sqrt{2\,\mathrm{i}}\;k\,\mathcal{F}(k,\zeta)\,, \tag{31}$$

$$\int \frac{\tau\,\mathrm{d}\tau}{\sqrt{(\tau_f-\tau)(1+\tau^2)}} \;=\; \sqrt{2\,\mathrm{i}}\;k\,\left[\,\tau_f\,\mathcal{F}(k,\zeta) - (\tau_f+\mathrm{i})\mathcal{E}(k,\zeta)\,\right]\,, \tag{32}$$

where

$$k \;=\; \sqrt{\frac{2\,\mathrm{i}}{\tau_f+\mathrm{i}}}\,, \qquad \zeta \;=\; \sqrt{\frac{1-\mathrm{i}\,\tau}{2}}\,. \tag{33}$$

However, this approach is difficult to implement, since standard algorithms for the evaluation of $\mathcal{F}$ and $\mathcal{E}$ are based on the assumption of a real variable and parameter. We rely instead on a direct treatment of equations (29)–(30).

5.2 Transformation of the integrals

For brevity, we set $p = \tau_i$ and $q = \tau_f - \tau_i$. Writing $\tau = p + q\,u$ with $u \in [\,0, 1\,]$, equations (29)–(30) can be re–formulated so that the integrals have fixed limits. This yields the equations

$$f(p,q) \;:=\; \int_0^1 \frac{\mathrm{d}u}{\sqrt{1-u}\,\sqrt{1+(p+qu)^2}} \;-\; 2\,(1-\delta/L) \;=\; 0\,, \tag{34}$$

$$g(p,q) \;:=\; \int_0^1 \frac{(p+qu)\,\mathrm{d}u}{\sqrt{1-u}\,\sqrt{1+(p+qu)^2}} \;=\; 0\,, \tag{35}$$

in p and q. In general, numerical methods must be employed to solve these equations. The Newton–Raphson iteration requires the partial derivatives of f and g, which may be expressed as

$$f_p(p,q) \;=\; -\int_0^1 \frac{(p+qu)\,\mathrm{d}u}{\sqrt{1-u}\,[\,1+(p+qu)^2\,]^{3/2}}\,, \tag{36}$$

$$f_q(p,q) \;=\; -\int_0^1 \frac{u(p+qu)\,\mathrm{d}u}{\sqrt{1-u}\,[\,1+(p+qu)^2\,]^{3/2}}\,, \tag{37}$$

$$g_p(p,q) \;=\; \int_0^1 \frac{\mathrm{d}u}{\sqrt{1-u}\,[\,1+(p+qu)^2\,]^{3/2}}\,, \tag{38}$$

$$g_q(p,q) \;=\; \int_0^1 \frac{u\,\mathrm{d}u}{\sqrt{1-u}\,[\,1+(p+qu)^2\,]^{3/2}}\,. \tag{39}$$

The integrals in (34)–(35) and (36)–(39) can be evaluated to any desired precision by a suitable numerical quadrature scheme, but diligence is required to ensure satisfactory results. These integrals are all of the form

$$I \;=\; \int_0^1 \frac{h(u)}{\sqrt{1-u}}\,\mathrm{d}u\,, \tag{40}$$

where the functions $h(u)$ are non–singular on $u \in [\,0, 1\,]$. Since the integrands are unbounded as $u \to 1$, the direct application of numerical quadrature rules does not yield accurate results. To circumvent this problem, the integrals can be decomposed as

$$I \;=\; \int_0^1 \frac{h(u)-h(1)}{\sqrt{1-u}}\,\mathrm{d}u \;+\; \int_0^1 \frac{h(1)}{\sqrt{1-u}}\,\mathrm{d}u\,. \tag{41}$$

Here the integrand of the first term,

$$J \;:=\; \int_0^1 \frac{h(u) - h(1)}{\sqrt{1-u}}\, \mathrm{d}u\,, \tag{42}$$

is non–singular, since by l'Hôpital's rule it has the limiting value 0 as $u \to 1$. The integral (42) is therefore better suited to numerical quadrature. Note also that the second term in (41) has the simple exact value

$$\int_0^1 \frac{h(1)}{\sqrt{1-u}}\, \mathrm{d}u \;=\; 2\, h(1)\,.$$

5.3 Numerical quadrature scheme

A numerical quadrature rule estimates the integral of a function $\phi(u)$ over an interval $u \in [\, a, b\,]$ as a weighted sum of discrete values $\phi(u_i)$, sampled at nodes $u_1, \ldots, u_N \in [\, a, b\,]$. Well–known examples include the Gaussian and Newton–Cotes quadrature rules. A key requirement, in the present context, is the ability to efficiently achieve any desired accuracy through simple rules for successively densifying the node set $u_1, \ldots, u_N$. The composite Simpson rule admirably serves this need, and is very easy to implement.

For uniformly–space nodes $u_i = i/N$, $i = 0, \ldots, N$ (where N is even), the composite Simpson rule quadrature formula estimates the integral (42) as

$$J \;\approx\; \frac{1}{3N} \sum_{i=1}^{N/2} w(u_{2i-2}) + 4\, w(u_{2i-1}) + w(u_{2i})\,, \tag{43}$$

where we set

$$w(u) \;:=\; \frac{h(u) - h(1)}{\sqrt{1-u}}\,.$$

Choosing $N = 2^n$ for $n = 1, 2, \ldots$, one can re–use the previously–computed w values on increasing n to $n+1$, to formulate an efficient, rapidly–convergent method. Table 1 illustrates the rapid convergence of the composite Simpson rule quadrature values (43) for the functions (34)–(35) and (36)–(39), when $p = 0.2$ and $q = -0.4$. It can be shown that the error ϵ in the estimates of these integrals satisfies the bound

$$|\epsilon| \;<\; \frac{1}{180 N^4} \max_{u \in [\,0,1\,]} |w^{(4)}(u)|\,.$$

n	f	f_p	f_q	g	g_p	g_q
1	0.37947007	0.13650015	0.16792902	-0.14196016	1.93959849	1.31104963
2	0.38094052	0.13073230	0.15846683	-0.13512882	1.94370025	1.29868088
3	0.38145473	0.12859954	0.15501024	-0.13267627	1.94517054	1.29408413
4	0.38163359	0.12783445	0.15378903	-0.13180477	1.94568487	1.29242857
5	0.38169617	0.12756233	0.15335870	-0.13149603	1.94586515	1.29183839
6	0.38171817	0.12746585	0.15320690	-0.13138677	1.94592858	1.29162891
7	0.38172592	0.12743170	0.15315330	-0.13134813	1.94595094	1.29155471
8	0.38172866	0.12741961	0.15313436	-0.13133446	1.94595884	1.29152845
9	0.38172963	0.12741534	0.15312767	-0.13132963	1.94596163	1.29151916
10	0.38172997	0.12741383	0.15312530	-0.13132792	1.94596261	1.29151588
11	0.38173009	0.12741329	0.15312446	-0.13132732	1.94596296	1.29151471
12	0.38173013	0.12741310	0.15312417	-0.13132711	1.94596309	1.29151430
13	0.38173015	0.12741304	0.15312406	-0.13132703	1.94596313	1.29151416
14	0.38173015	0.12741301	0.15312403	-0.13132700	1.94596315	1.29151411
15	0.38173016	0.12741301	0.15312401	-0.13132699	1.94596315	1.29151409
16	0.38173016	0.12741300	0.15312401	-0.13132699	1.94596315	1.29151408
17	0.38173016	0.12741300	0.15312401	-0.13132699	1.94596315	1.29151408
18	0.38173016	0.12741300	0.15312401	-0.13132699	1.94596315	1.29151408

Table 1: Variation of composite Simpson rule quadrature values with $n = \log_2 N$ for the functions (34)–(35) and (36)–(39) when $p = 0.2$, $q = -0.4$.

5.4 Newton–Raphson iteration

From an initial estimate (p_0, q_0) the Newton–Raphson iteration computes an iterated sequence of approximations

$$(p_k, q_k) \;=\; (p_{k-1}, q_{k-1}) \;+\; (\delta p, \delta q)\,, \quad k = 1, 2, \ldots\,,$$

to the solution of equations (34)–(35). The increments $(\delta p, \delta q)$ at iteration k are the solutions of the linear system

$$\begin{bmatrix} f_p & f_q \\ g_p & g_q \end{bmatrix} \begin{bmatrix} \delta p \\ \delta q \end{bmatrix} \;=\; - \begin{bmatrix} f \\ g \end{bmatrix}\,,$$

where it understood that f, f_p, f_q, g, g_p, g_q are evaluated at (p_{k-1}, q_{k-1}).

To estimate a starting approximation (p_0, q_0), the base curve is modelled as a circular arc of radius r, subtended by angle 2θ, between the points $(0, 0)$

and $(1-\delta/L, 0)$ in the (x, z) plane. Here, the parameters r and θ must obey the constraints

$$2\,r\theta \;=\; L \quad \text{and} \quad 2\,r\sin\theta \;=\; L-\delta\,,$$

and consequently θ must satisfy

$$\sin\theta \;=\; (1-\delta/L)\,\theta\,.$$

Hence, using the truncated Taylor series approximation $\sin\theta \approx \theta - \frac{1}{6}\,\theta^3$, we obtain

$$\theta \;\approx\; \sqrt{6\delta/L}\,.$$

Since the end tangents of the circular arc are $(\tau_i, \tau_f) = (\tan\theta, -\tan\theta)$ we set $(p_0, q_0) \;=\; (\tan\theta, -2\tan\theta)$. This starting approximation is satisfactory for small δ/L ($\lesssim 0.25$), and the residual $|f(p,q)|$ and $|g(p,q)|$ values are typically suppressed below 10^{-12} after just 4 or 5 Newton–Raphson iterations.

However, when computing p, q for a sequence of increasing δ/L values, it is preferable to use the converged p, q for the previous δ/L as the starting approximation for the subsequent δ/L. This yields faster convergence (within just 2 or 3 iterations) and greater certainty of convergence when $\delta/L > 0.25$. Table 2 lists the p, q values and corresponding tangent angles α_i, α_f computed in this manner for $0.025 \le \delta/L \le 0.500$ in increments of 0.025 — these values are also illustrated graphically in Figures 6 and 7.

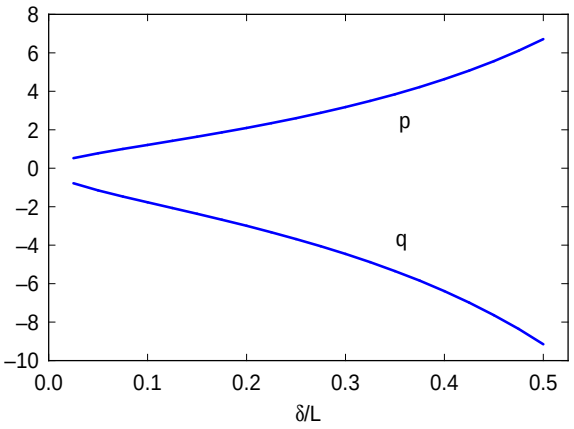

Figure 6: Variation of the parameters p and q with δ/L.

δ/L	p	q	α_i	α_f
0.025	0.5243253583	-0.7809938038	27.669162°	−14.395274°
0.050	0.7778872476	-1.1508868819	37.878891°	−20.455497°
0.075	0.9998865098	-1.4697646018	44.996749°	−25.167803°
0.100	1.2123148217	-1.7709385326	50.481861°	−29.188761°
0.125	1.4239466441	-2.0676681441	54.920649°	−32.770255°
0.150	1.6396782650	-2.3672876799	58.621998°	−36.039989°
0.175	1.8628704135	-2.6747596758	61.772830°	−39.072775°
0.200	2.0962032592	-2.9939733431	64.496385°	−41.916546°
0.225	2.3420670364	-3.3283365410	66.878814°	−44.603937°
0.250	2.6027749865	-3.6810960671	68.982959°	−47.158158°
0.275	2.8807004966	-4.0555408939	70.856180°	−49.596254°
0.300	3.1783814389	-4.4551535296	72.535093°	−51.931060°
0.325	3.4986129117	-4.8837414267	74.048604°	−54.172423°
0.350	3.8445408178	-5.3455668766	75.419930°	−56.328013°
0.375	4.2197652928	-5.8454884115	76.667988°	−58.403874°
0.400	4.6284621407	-6.3891251708	77.808384°	−60.404818°
0.425	5.0755311714	-6.9830564347	78.854131°	−62.334699°
0.450	5.5667823740	-7.6350711228	79.816174°	−64.196628°
0.475	6.1091743705	-8.3544866547	80.703797°	−65.993131°
0.500	6.7111250457	-9.1525637957	81.524924°	−67.726261°

Table 2: Variation of the parameters p, q and tangent angles α_i, α_f with δ/L.

5.5 Base curve geometry

Once the p, q parameters are computed, the shape of the sail base curve can be determined. To accomplish this, the relation (27) is inverted to express the tangent $\tau = \tan\alpha$ in terms of the arc length s as

$$\tau \;=\; \tau_f \;-\; (\tau_f - \tau_i)(1 - s/L)^2 \;=\; p + q \;-\; q(1 - s/L)^2\,. \qquad (44)$$

Thus, using $\mathrm{d}x/\mathrm{d}s = \cos\alpha$, $\mathrm{d}z/\mathrm{d}s = -\sin\alpha$ and the relations (28), the arc–length parameterization $\mathbf{c}(s) = (x(s), z(s))$ of the base curve has the integral

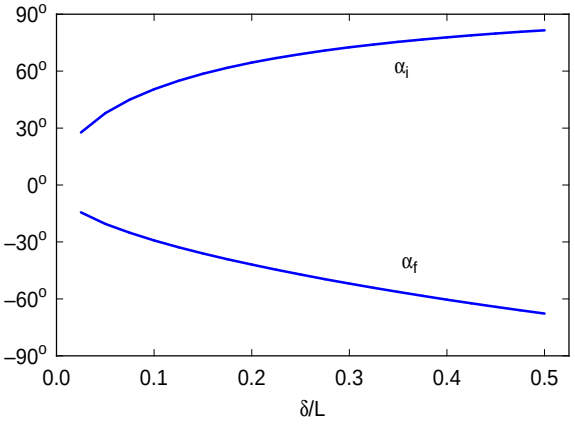

Figure 7: Variation of the base curve tangent angles α_i, α_f with δ/L.

representation

$$x(s) \;=\; \int_0^s \frac{\mathrm{d}\xi}{\sqrt{1+[\,p+q-q(1-\xi/L)^2\,]^2}}\,,$$
$$z(s) \;=\; -\int_0^s \frac{[\,p+q-q(1-\xi/L)^2\,]\,\mathrm{d}\xi}{\sqrt{1+[\,p+q-q(1-\xi/L)^2\,]^2}}\,.$$

The forms defining $x(s)$, $z(s)$ are again (incomplete) elliptic integrals. Since the integrands are non–singular, the Simpson rule quadrature may be applied with uniform nodes $\xi_1, \ldots, \xi_N \in [\,0, s\,]$ to evaluate them. Alternatively, by differentiating these expressions, a standard (e.g., 4th–order Runge–Kutta) scheme may be employed to integrate the resulting differential equations with suitable steps in the arc length s between 0 and L.

Figure 8 illustrates the computed base curve shape for the cases $\delta/L =$ 0.025, 0.05, 0.1, 0.2, 0.3, 0.4, and 0.5. Note that the base curve is distinctly asymmetric, with a steeper tangent angle at $x = 0$ than at $x = L - \delta$ (as indicated in Table 2). Note also that equation (44) defines an exact relation between the tangent $\tau = \tan\alpha$ and the arc length s along the base curve, facilitating the integrations required to determine the total solar radiation forces and moments on a billowed sail.

For practical use, it might be preferable to pre–compute and store the p and q values corresponding to a sufficiently dense sampling of δ/L, and then invoke an interpolation scheme to estimate intermediate values — this is a

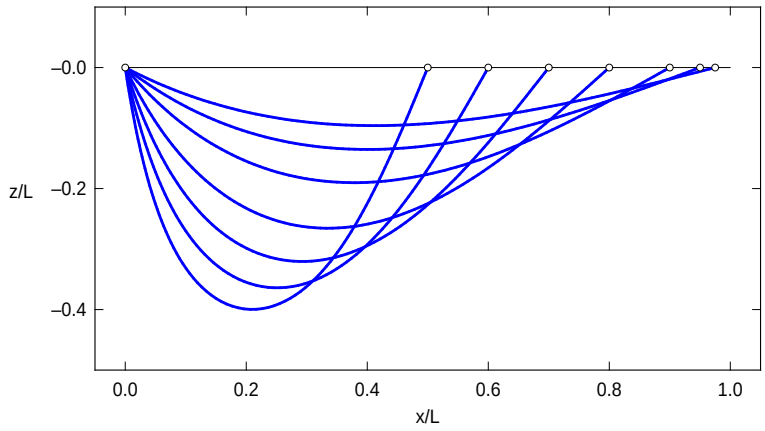

Figure 8: Sail base curve shape for $\delta/L = 0.025, 0.05, 0.1, 0.2, 0.3, 0.4, 0.5$.

common methodology for the efficient evaluation of transcendental functions to a prescribed precision. The smooth variation of p, q with δ/L (see Figure 6) suggests that this can yield high accuracy without the cost of iterating over numerical quadratures for each δ/L.

6 Discussion

A quantitative analysis of the mechanics of a bounded inextensible solar sail membrane wing has been presented. A key component of this analysis is the parameterization of the sail surface as a developable ruled surface, with the developability condition being expressed as the constraint (3) satisfied by the base curve $\mathbf{c}(s)$ and ruling direction $\mathbf{d}(s)$. This condition can be regarded as a two–dimensional generalization of the governing equation for an inextensible chain. Moreover, the parameterization allows one to take advantage of the invariant direction of the SRP force along each ruling. The force and moment equations can then be formulated for an element bounded by two neighboring rulings, yielding the univariate equilibrium equations (10) and (18).

The parameterization also facilitates integrations over the entire surface by expressing the ruling parameter integration limit in terms of the base curve parameter. For the right–triangle sail wing considered herein, the t integration limit is $l(s)$. When the sail billows into a generalized cylinder surface we have $s + l(s) = L$, where L is the fixed length of the base curve

$\mathbf{c}(s)$ from O to P, so the integration range for t is simply 0 to $L - s$. Many physical quantities of interest that require integration over the entire surface, such as total surface SRP force, moment about the center, etc., can thus be easily computed based on the presented solution.

The simplifying assumptions concerning the sail membrane mechanics adopted herein facilitate a rigorous study of the idealized case of inextensible membranes subject to SRP. In this ideal case, the membrane thickness is negligible compared to its overall dimensions, and the membrane cannot support any bending or torsional loads. These assumptions may no longer be appropriate for thick membranes, for which one may need to accommodate bending and torsional stresses in the equilibrium analysis. Also, the ideal case considers only specular SRP reflection, yielding forces that act in the surface normal direction, and it is assumed that the surface reflectivity is homogeneous and does not degrade with time. These assumptions may be invalidated by manufacturing variations or environmental factors, in which case the analysis would need to specifically account for them.

Several other observations arise from this study. The moment vector $d\mathbf{r}$ in equation (11) makes only a higher–order contribution to the total torque, and may therefore be neglected. Thus, finding the exact location of the center of pressure on the differential sub–element — a task that incurs significant analytical effort — is unnecessary. Also, the introduction of the unit vector $\mathbf{e} = \mathbf{d}'/|\mathbf{d}'|$ greatly simplifies the analysis, since using the explicit derivative of $\mathbf{d}'/|\mathbf{d}'|$ is cumbersome and hinders interpretation. Although the base curve geometry can be expressed in terms of standard elliptic integrals, they incur complex variables and parameters, and singular integrands, which complicate the solution of the boundary value problem. However, by appropriate transformations of the integrals, the boundary value problem can be solved to any desired precision in real arithmetic using simple numerical quadrature rules. This is much more efficient and accurate than the numerical optimization algorithms presented in [8], and the present method allows one to find the base curve for any given boundary conditions. Finally, although this study considers only steady state equilibrium, it can be readily extended to encompass a complete dynamical theory of bounded inextensible membranes. Such a theory may also be of interest in other engineering applications.

7 Conclusion

A rigorous analysis of the equilibrium mechanics of inextensible membranes subject to solar radiation pressure and given boundary constraints has been presented. The inextensibility condition and the force and torque balance equations yield a system of constraints that govern the shape of the billowed membrane sail wing for a specified tip displacement. These constraints yield the (non–obvious) conclusion that the resulting equilibrium sail shape is a generalized cylinder, i.e., a ruled surface whose rulings are all parallel to each other. The geometry of the base curve as a solution to the boundary value problem is also given, with accompanying numerical results.

Acknowledgment

This research has been partially supported by the N. & M. Sarigul–Klijn Space Engineering/Flight Research award.

References

[1] M. Bergou and M. Wardetzky, A quadratic bending model for inextensible surfaces, Eurographics Symposium on Geometry Processing, 2006, pp. 227–230.

[2] J. Block, M. Straubel, and M. Wiedemann. Ultralight deployable booms for solar sails and other large gossamer structures in space, *Acta Astronautica* 68 (2011), 984–992.

[3] M. A. Brown and G. Henshaw, Technology requirements for large, ultra–light solar sails, in: 2nd International Symposium on Solar Sailing, New York, 2010.

[4] R. Burton, UltraSail — ultra–lightweight solar sail concept, in: 41st AIAA/ASME/SAE/ASEE Joint Propulsion Conference, Tucson, AZ, 2005, pp. 1–14.

[5] M. Chen and K. Tang, A fully geometric approach for developable cloth deformation simulation, *The Visual Computer* 26 (2010), 853–863.

[6] R. W. Dickey, Equilibrium states of inextensible membranes under gravity, *Journal of Elasticity* 76 (2004), 67–88.

[7] B. Fu and F. O. Eke, Attitude control methodology for large solar sails, *Journal of Guidance, Control, and Dynamics* 38 (2014), 662–670.

[8] B. Fu and F. O. Eke, Further investigation of the body torques on a square solar sail due to the displacement of the sail attachment points, *Aerospace Science and Technology* 50 (2016), 281–294.

[9] C. E. Garner, Large area sail design concepts, in: IEEE 2000 Aerospace Conference Proceedings, 2000, pp. 447–457.

[10] J. He, S. P. Gong, J. F. Li, A curved surface solar radiation pressure force model for solar sail deformation, *Science China — Physics, Mechanics, and Astronomy* 55 (2012), 141–155.

[11] J. He, S. P. Gong, J. F. Li, and Y. Liu, The solar radiation pressure force models for a general sail surface shape, in: *Advances in Solar Sailing* (M. McDonald, ed.), Springer, 2014, pp. 469-488.

[12] S. S. Ligarò and R. Barsotti, Equilibrium shapes of inflated inextensible membranes, *International Journal of Solids and Structures* 45 (2008), 5584–5598.

[13] R. H. MacNeal, J. M. Hedgepeth, and H. U. Schuerech, Heliogyro solar sailer: summary report, NASA Technical Report, 1969.

[14] L. E. Malvern, *Introduction to the Mechanics of a Continuous Medium*, Prentice–Hall, Englewood Cliffs NJ, 1969.

[15] C. R. McInnes, *Solar Sailing: Technology, Dynamics and Mission Applications*, Springer, 2004.

[16] M. Perriollat and A. Bartoli, A computational model of bounded developable surfaces with application to image–based three–dimensional reconstruction, *Computer Animation and Virtual Worlds* 24 (2013), 457–475.

[17] H. Sakamoto, Y. Miyazaki, and K. C. Parkt, Finite element modeling of sail deformation under solar radiation pressure, *Journal of Spacecraft and Rockets* 44 (2007), 514–521.

[18] D. J. Struik, *Lectures on Classical Differential Geometry*, Dover (reprint), New York, 1961.

[19] Y. Tsuda, O. Mori, R. Funase, H. Sawada, T. Yamamoto, T. Saiki, T. Endo, and J. Kawaguchi, Flight status of IKAROS deep space solar sail demonstrator, *Acta Astronautica* 69 (2011), 833–840.

[20] B. Wie, Solar sail attitude control and dynamics, Part 1, Journal of Guidance, Control, and Dynamics 27 (2004), 526–535.

[21] B. Woo, K. M. Ertmer, V. L. Coverstone, R. L. Burton, G. F. Benavides, and D. L. Carroll, Deployment experiment for ultralarge solar sail system (UltraSail), *Journal of Spacecraft and Rockets*, 48 (2011), 874–880.

[22] T. Yamaguchi, Y. Mimasu, Y. Tsuda, H. Takeuchi, and M. Yoshikawa, Estimation of solar radiation pressure force for solar sail navigation, in: Proceedings of the 61st International Astronautical Congress, IAC–10.C1.6.4, 2010.

[23] D. Yong, Strings, chains, and ropes, *SIAM Review* 48 (2006), 771–781.